

Self-assembly of monodisperse clusters: Dependence on target geometry

Alex W. Wilber,¹ Jonathan P. K. Doye,^{1,*} and Ard A. Louis²

¹*Physical and Theoretical Chemistry Laboratory, University of Oxford,
South Parks Road, Oxford OX1 3QZ, United Kingdom*

²*Theoretical Physics, University of Oxford, Keble Road, Oxford OX1 3NP, United Kingdom*
(Dated: December 23, 2008)

Future advances in nanotechnology will require a detailed understanding of the self-assembly of anisotropic particles, and its dependence on the details of the subunits and on the target structure. We apply a simple model system of patchy particles to study monodisperse self-assembly, using the Platonic solids as targets. We find marked differences between the assembly behaviours of the targets; tetrahedra, octahedra and icosahedra assemble easily, while cubes are more challenging and dodecahedra will not assemble. We relate these differences to the kinetics and thermodynamics of assembly, and study the competition arising from stable and metastable aggregates. Finally we make some predictions regarding what classes of structure represent feasible self-assembly targets: in particular, we suggest that targets with triangular faces will tend to be the easiest structures to assemble.

PACS numbers: Don't know

I. INTRODUCTION

The assembly of nano-structured materials and devices presents a great challenge for the future. A very promising approach is offered by self-assembly processes, in which nanoscopic or colloidal building blocks come together spontaneously to form ordered structures. While top-down approaches to assembly become increasingly challenging on small lengthscales, self-assembly offers a bottom-up approach which circumvents many of these difficulties, while providing its own unique challenges in the synthesis and design of the subunits.

Current examples of synthetic self-assembling systems, such as micelles and block copolymers, lead to polydisperse and imperfectly controlled products. Biological systems, by contrast, display an astonishing variety of ordered and precise self-assembly processes. For example, the process of virus replication involves the assembly of hundreds of proteins to form highly symmetric and monodisperse shells (capsids). Such systems provide an inspiring example of the level of control possible in self-assembly. Future applications in nanotechnology are likely to require this level of sophisticated control in order to form precisely ordered structures.

One attractive aspect of self-assembly is the idea that the structure of the final product is entirely determined by the interactions between the subunits (along with the reaction conditions) so that, given complete understanding of the principles of self-assembly, the subunits can be carefully designed to produce a given product. In order to implement these designs a great deal of control is required over the structure of the subunits. One key requirement for sophisticated self-assembly is the production of anisotropic subunits, which only attract each other in certain directions. Rational design of this anisotropy then allows for control over the resultant self-assembled structures.

Recently there has been a great deal of progress in syn-

thesising such anisotropic subunits. Stellacci et al have produced patterned spherical colloids.

The production of functional self-assembling systems will require not only advanced synthesis techniques to produce the subunits, but also a strong theoretical understanding of the self-assembly process so that appropriate designs and conditions can be chosen. Recently there has been significant progress in simulating monodisperse self-assembly^{1–10}. However, these simulations have mostly focussed on the self-assembly of viruses, and so include protein-like interactions which are more specific than those which are likely to be available in the first generation of synthetic anisotropic subunits.

Here we consider a minimal patchy particle model, representing colloids or nanoparticles with anisotropic interactions. Our model is intentionally simple, so that we are easily able to observe and study behaviours which we expect to be general properties of monodisperse self-assembly rather than being specific to our model. Our patchy particle model is similar to those used in a different context to study the properties of low density fluids and gels^{11,12}.

We build on earlier work¹³ to consider the assembly of a set of simple assembly targets, the Platonic solids. In particular we are interested to understand what properties of the constituent particles lead to successful assembly, and how the choice of target structure affects the success and the mechanism of assembly. As a result we are able to make predictions as to what classes of structure are likely to be feasible self-assembly targets, given simple interactions between subunits. We also seek to characterise the main processes which compete with successful assembly, the structures they lead to, and how their impact on yield can be minimised. We hope that this work may offer some guidance to experimental groups seeking to make practical synthetic self-assembling systems.

The assembly process studied here is strongly reminiscent of that of virus capsids, in that anisotropic particles

come together to form closed, highly symmetric structures. However, the interaction potential we use has no dependence on the torsional angle between interacting particles. While this is a good choice for modelling synthetic anisotropic particles, it is not a good representation of the interactions between virus capsomers, and leads to behaviour not observed for systems of virus capsomers. We consider a model including torsional interactions, and hence more closely mirroring capsid assembly, in the accompanying paper.

II. METHODS

A. Model

We make use of a minimal model, designed to contain only the essential features required for targeted self-assembly, while allowing for efficient simulation. The model consists of spherical particles patterned with attractive patches. They are described by a modified Lennard-Jones potential, in which the repulsive part of the potential is isotropic as usual, but the attractive part is anisotropic and depends on the alignment of patches on interacting particles. Specifically, the potential is described by

$$V_{ij}(\mathbf{r}_{ij}, \mathbf{\Omega}_i, \mathbf{\Omega}_j) = \begin{cases} V_{LJ}(r_{ij}) & r < \sigma_{LJ} \\ V_{LJ}(r_{ij}) V_{\text{ang}}(\hat{\mathbf{r}}_{ij}, \mathbf{\Omega}_i, \mathbf{\Omega}_j) & r \geq \sigma_{LJ}, \end{cases} \quad (1)$$

where V_{LJ} is the Lennard-Jones potential, given by

$$V_{LJ}(r) = 4\epsilon \left[\left(\frac{\sigma_{LJ}}{r} \right)^{12} - \left(\frac{\sigma_{LJ}}{r} \right)^6 \right]. \quad (2)$$

V_{ang} is an angular modulation factor, which depends on the orientations of the patches on the two interacting particles, as well as the direction of the vector joining them. Specifically,

$$V_{\text{ang}}(\hat{\mathbf{r}}_{ij}, \mathbf{\Omega}_i, \mathbf{\Omega}_j) = G_{ij}(\hat{\mathbf{r}}_{ij}, \mathbf{\Omega}_i) G_{ji}(\hat{\mathbf{r}}_{ji}, \mathbf{\Omega}_j), \quad (3)$$

$$G_{ij}(\hat{\mathbf{r}}_{ij}, \mathbf{\Omega}_i) = \exp \left(-\frac{\theta_{k_{\min}ij}^2}{2\sigma^2} \right), \quad (4)$$

where σ_{ang} gives the width of the Gaussian, θ_{kij} is the angle between patch vector k on particle i and the interparticle vector \mathbf{r}_{ij} , and k_{\min} is the patch that minimizes the magnitude of this angle. Hence, only the patches on each particle that are closest to the interparticle axis interact with each other.

A particular particle design is specified simply by a set of unit vectors describing the positions of the attractive patches. For each of our target structures there is an associated particle design, in which the patches are placed such that they point directly at the neighbouring particles in the target structure. Fig. 1 shows the component particles and complete clusters for each of our target structures, the Platonic solids.

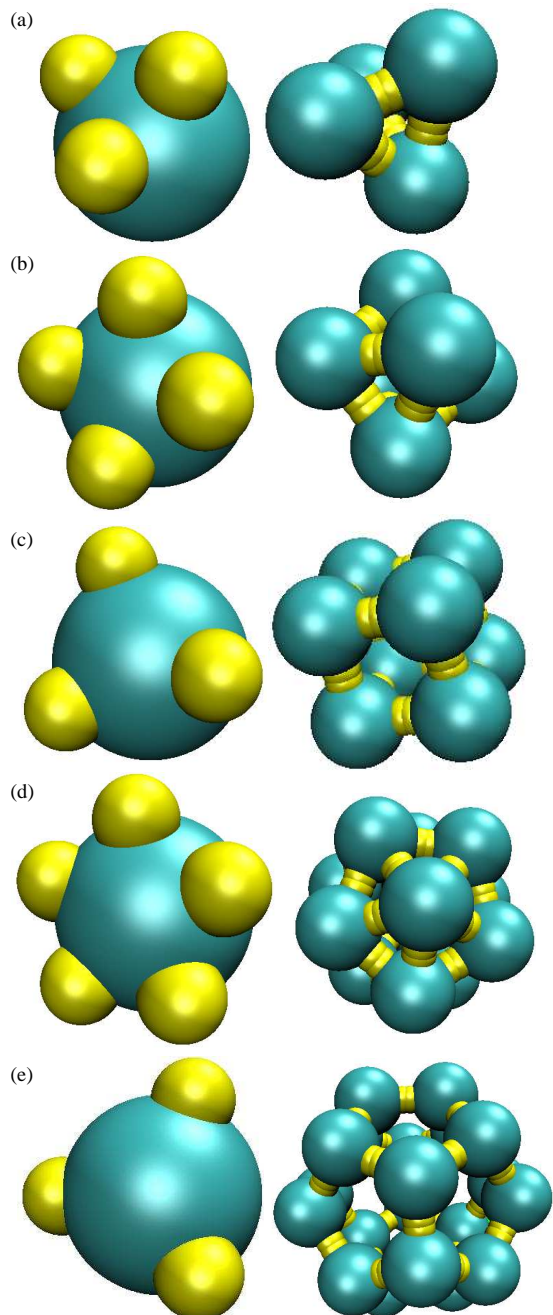


FIG. 1: (Colour Online) Single particles and complete clusters for (a) tetrahedra, (b) octahedra, (c) cubes, (d) icosahedra and (e) dodecahedra. The yellow spheres mark the positions of the patch vectors, and have no excluded volume of their own.

B. Simulation methods

1. Use of Metropolis Monte Carlo for studying dynamics

Our simulations consist of Metropolis Monte Carlo (MC) simulations in the canonical ensemble, using pe-

riodic boundary conditions. The allowed move types are small single-particle translations and rotations. The translational moves are randomly chosen from a cube centred on the selected particle. Rotational moves make use of a quaternion description of the particle's orientation; the proposed quaternion is given by the renormalised sum of the current quaternion and a smaller, randomly generated 4-vector.

This method does not directly simulate the physical trajectories of the particles, and is more often used to obtain thermodynamic averages of the properties of a system. However, the restriction to small moves results in the system approximating diffusive dynamics^{??}. This method has the advantage of being very efficient, since derivatives of the potential (which are expensive to calculate) are not required.

This use of single-particle moves rather than cluster moves can cause large clusters to move unphysically slowly. For systems where cluster migration is an important part of the dynamics, the use of single-particle moves can lead to significant errors. However, we believe that for the systems studied here cluster migration is not a very important process, and further, the relatively soft potentials we have used mitigate the difficulty and still allow clusters to move reasonably quickly. Indeed, preliminary simulations using the VMMC cluster-move algorithm show few differences to our single-particle-move results.

2. Assignment of clusters and rings

Many of our results make use of information on the clusters present in the simulations, and of the rings present within those clusters. We define two particles as being bonded if their interaction energy satisfies $V_{ij} \leq -0.4$. Particles are part of the same cluster if they are connected by an unbroken chain of bonds. We identify target clusters by matching the number of particles and bonds in the cluster to the profile for the target cluster, including some allowance for bonds temporarily weakened by thermal fluctuation. We define rings using the shortest-path algorithm given in Ref. ??; a closed loop is counted as a ring if there is no pair of particles on the ring connected by any chain of bonds shorter (i.e. consisting of fewer bonds) than the route by which they are connected along the ring.

3. Umbrella sampling

The conventional Monte Carlo moves described above do not tend to give good equilibrium statistics in a short time-frame. To improve the sampling where equilibrium data is needed we make use of umbrella sampling. The essential idea is to bias the system such that free energy barriers are easier to cross, thus allowing the system to explore phase space much more quickly. Under

this scheme, instead of choosing the acceptance probabilities using a Boltzmann distribution, we use the modified distribution $\exp[-\beta(\mathcal{V} + w(Q))]$, where Q is an order parameter and $w(Q)$ is a weighting function. Canonical averages are simple to obtain from a simulation of such a non-Boltzmann (nB) ensemble using the expression

$$\langle B \rangle_{NVT} = \langle B \exp[\beta w(Q)] \rangle_{\text{nB}}, \quad (5)$$

where B is some generic property of the system.

Both the order parameter and the weighting function need to be chosen carefully for a given system. In our equilibrium simulations we consider the transition from a gas of monomers and small clusters to completed target structures. Because complete clusters exert only very weak attractions on one another, simulation of single-cluster systems gives a good approximation to the thermodynamics of bulk systems. This choice of system allows us to make use of a convenient order parameter, given by the number of particles in the largest cluster in the simulation. By favouring intermediate values of this order parameter (which are high in free energy) we are able to greatly facilitate exchange between the monomer gas and the target cluster, and hence obtain good statistics. The weighting function $w(Q)$ was set by iteratively performing simulations and improving $w(Q)$ until the time spent at each value of Q was approximately equal.

In the case of the dodecahedron we found that the above order parameter was inadequate, and we instead used two order parameters simultaneously, with the weighting function $w(Q_1, Q_2)$ being a function of both. Here Q_1 and Q_2 were given by the number of bonds and the number of pentagons respectively in the largest cluster (see Section II B 2). This method was combined with Hamiltonian exchange (see below) to obtain equilibrium statistics.

4. Hamiltonian exchange

In attempting to obtain equilibrium statistics for the formation of a single dodecahedron, we were unable to find any set of order parameters which would drive the system to successful assembly while using the potential described in Section II A. However, an alternative potential which included torsional constraints on the attraction between particles was known to lead to successful assembly (see Other Paper). This potential incorporates an additional factor into the attractive regime of the potential, given by

$$V_{\text{tor}} = \exp\left(-\frac{\theta_{\text{tor}}}{2\sigma_{\text{tor}}^2}\right), \quad (6)$$

where θ_{tor} is a measure of the torsional angle between the two particles, chosen such that $\theta_{\text{tor}} = 0$ in the target structure (more details are given in ref. Other Paper). As σ_{tor} approaches infinity, this potential converges on that described in Section II A.

In the parallel tempering method, an array of simulations are run in parallel, each at a different temperature, with stochastic exchange of configurations between the simulations. This allows even low temperature simulations to overcome kinetic barriers, by receiving configurations on the far side of those barriers from higher temperature simulations. Analogously, we used arrays of simulations where the differentiating factor was the potential (i.e. the Hamiltonian) rather than the temperature. One simulation had $\sigma_{\text{tor}} = \infty$, and hence gave equilibrium data for the potential described in Section II A, while a further 19 simulations had finite and decreasing values of σ_{tor} , down to the lowest at $\sigma_{\text{tor}} = 1.25$. The values in between were chosen adaptively to maximise the rate of configuration exchange between them. The low- σ_{tor} simulations allowed the system to reach the correctly assembled dodecahedron, and these configurations were stochastically passed back to the infinite- σ_{tor} simulation which sampled them appropriately.

We set the probability of each move being a configuration-swap attempt to 0.1. The acceptance probability is given by

$$p_{\text{acc}}((i, 1), (j, 2) \rightarrow (i, 2), (j, 1)) = \exp[\beta(W_{i,1} + W_{j,2} - W_{i,2} - W_{j,1})] \quad (7)$$

where i and j are Hamiltonians, and 1 and 2 are configurations. $W_{i,1}$ is the combined potential energy and umbrella weighting of configuration 1 with the Hamiltonian i , i.e. $W_{i,1} = V_i(\mathbf{r}_1^N) + w_i(Q(\mathbf{r}_1^N))$.

III. RESULTS

A. Overview

In this section we will survey the main features of our self-assembling system, identifying the region of parameter space in which assembly occurs, the transitions which define the boundary of this region, and the key differences between the behaviours of the various target structures. We will then proceed in the following sections to closely consider in turn the cluster-monomer gas transition, the cluster-liquid transition, the mechanisms of assembly and disassembly, and finally the anomalous behaviour of systems of dodecahedron-forming particles.

Throughout this paper we will have cause to compare the results of simulations performed with particles designed to form different target structures. For the sake of brevity we will refer to these simulations in a concise, if imprecise, manner; for example, when we refer to a “tetrahedral simulation”, we mean simply a simulation of particles designed to assemble into tetrahedra.

Because of the relative simplicity of our model, we are able to perform large numbers of simulations, and hence map out the assembly behaviour over a range of parameter space. Fig. 2 shows the yields of each of the platonic solids in simulations over a range of values of the temperature T and the patch width σ .

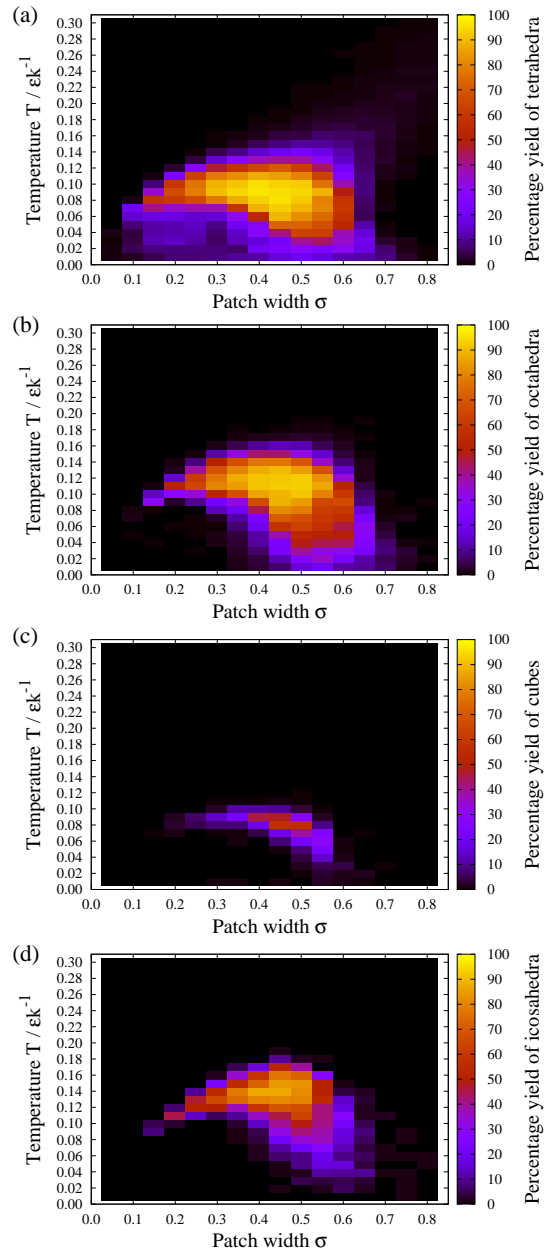


FIG. 2: (Colour Online) The percentage yield of target clusters formed after 80 000 MC cycles as a function of the patch width σ (measured in radians) and the temperature for 1200 particles at a number density of $0.15 \sigma_{\text{LJ}}^{-3}$, for (a) tetrahedra, (b) octahedra, (c) cubes and (d) icosahedra. No plot is included for dodecahedra, since no dodecahedra were successfully assembled under any conditions. The white lines show the thermodynamic transition temperature T_c for the transition from a gas of clusters to a gas of monomers, calculated for a one-cluster system (see Section III B).

Significant differences between the plots are immediately apparent. Tetrahedra, octahedra and icosahedra assemble readily over wide ranges of parameter space. By contrast, cubes are more difficult to assemble and are only formed in a smaller region of parameter space, while dodecahedra never form at all. We shall return to the reasons for these differences later. However, the same physical principles apply in each case, and as a result the general shapes of the plots are similar.

The region of successful assembly is determined by a number of constraints, both thermodynamic and kinetic. To begin with the first of the thermodynamic effects, we find that at high temperature T the stable state becomes a gas of monomers and small clusters, and target clusters are no longer formed. We designate the approximate temperature of this transition T_c , and T_c lines are marked on Fig. 2 (the precise definition we have used to obtain T_c is discussed in Section III B). A second thermodynamic constraint arises at high patch width σ , where the patches are so wide that the target clusters cease to be the stable state of the system. Each patch then becomes capable of interacting with more than one neighbour, and so the system can both lower its energy and raise its entropy by forming large, unstructured liquid-like droplets.

Both of these effects can be seen in Fig. 3, which shows the average cluster size for each target structure, again as a function of T and σ . At high T the average cluster size approaches unity, signifying a monomer gas, while at high σ the existence of a liquid phase results in clusters containing essentially all the particles in the simulation.

Kinetic constraints become important at low values of T and σ . At low T the system becomes unable to escape from incorrect configurations. Since it is very likely that some incorrect bonds will be formed during the assembly process this results in very low yields, and the system instead forms glassy kinetic aggregates. At low values of σ the patches are very narrow. Particles will only rarely be sufficiently well aligned to feel attractive interactions from their neighbours, and growth is suppressed.

Sandwiched in the middle of these regions of inhibited assembly is a region of parameter space in which the target is both thermodynamically stable and kinetically accessible; in this region good yields of the target structure are obtained.

These effects are summarised in Fig. 4, which shows schematically the different regions of parameter space and the lines which separate them.

We will now examine some features of the systems' behaviour in more detail.

B. The cluster-monomer gas transition

The plots in Fig. 2 show that T_c , the temperature above which the stable state is dominated by monomers rather than target clusters, increases with patch width σ regardless of the target structure. We can explain this by considering the free energies of the monomer and clus-

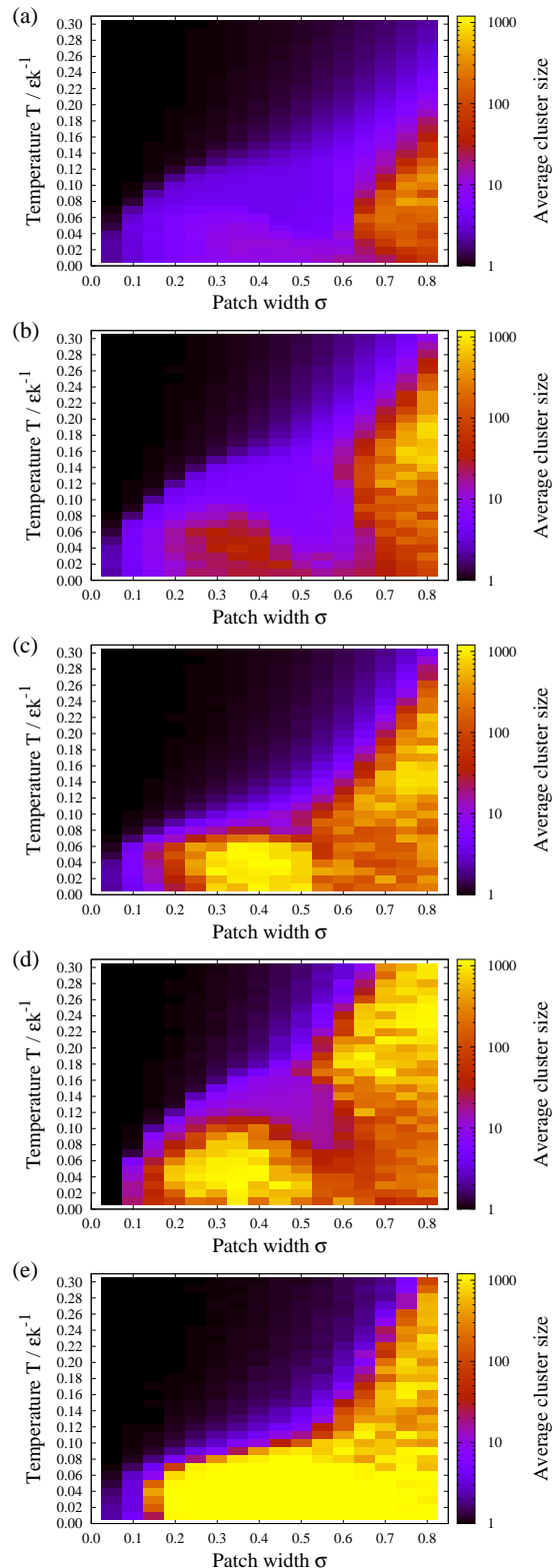


FIG. 3: (Colour Online) The mean cluster size (averaged over particles) of systems of particles designed to form (a) tetrahedra, (b) octahedra, (c) cubes, (d) icosahedra, and (e) dodecahedra, for the same simulations as Fig. 2. The white lines again show the thermodynamic transition temperature T_c for the transition from a gas of clusters to a gas of monomers, calculated for a one-cluster system (see Section III B).

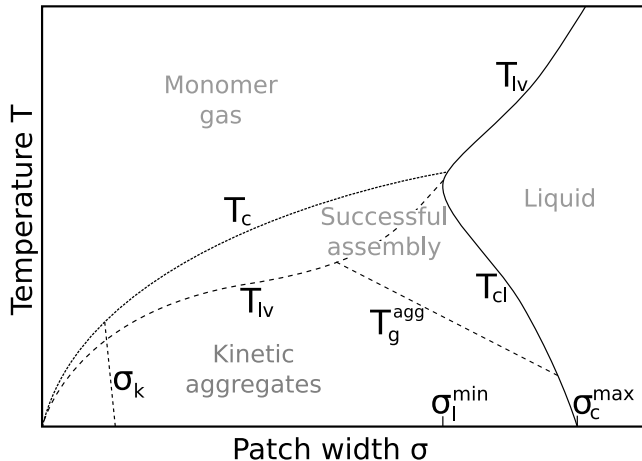


FIG. 4: A schematic diagram illustrating the regions of parameter space in which different behaviours are observed, and the interfaces between them. T_c is the approximate midpoint of the transition between the cluster gas and the monomer gas (see Section IIIB). T_{lv} and T_{cl} are the liquid-vapour phase transition lines for the monomer and cluster gases respectively. T_g^{agg} is the approximate temperature below which aggregates become unable to rearrange to form target clusters on the timescale of the simulations, and instead become trapped in a glass-like state. σ_k is the approximate value of σ below which the patches are so narrow that little assembly or aggregation is able to take place on the timescale of the simulations. σ_l^{\min} and σ_c^{\max} represent the lowest value of σ at which the liquid state is stable and the highest value of σ at which the cluster phase is stable respectively.

ter gases (we consider a state dominated by target clusters to be a gas, because the completed clusters have all patches pointing inwards and feel only very weak attractive forces). At T_c , A_m and A_c , the free energies of the monomer and cluster gases respectively, are approximately equal. A_m is largely independent of σ , as is the configurational energy per particle in the cluster gas, $V_c \approx \frac{m\epsilon}{2}$, where m is the number of patches per particle. However, the entropy S_c of the cluster gas increases with σ - at higher σ the clusters will be free to undergo larger vibrations, leading to a higher vibrational entropy.

While this is a generic feature, T_c otherwise shows strong target dependence. Fig. 5 shows the heat capacity C_v as a function of temperature for each of the target structures at $\sigma = 0.45$. The peaks in the C_v curves correspond to the cluster-monomer gas transition, and we define T_c as the temperature at which C_v is a maximum. It is important to note that these plots and the resulting values of T_c were obtained from small systems containing only sufficient particles to form one target cluster. As a result we expect significant finite size effects, and the values for bulk systems may be somewhat different. However, we expect the order of the C_v peaks to be unchanged in the bulk.

Note that the C_v plot for dodecahedra exhibits a distinct shoulder, which turns out to be very important. We shall return to this in Section IIIE.

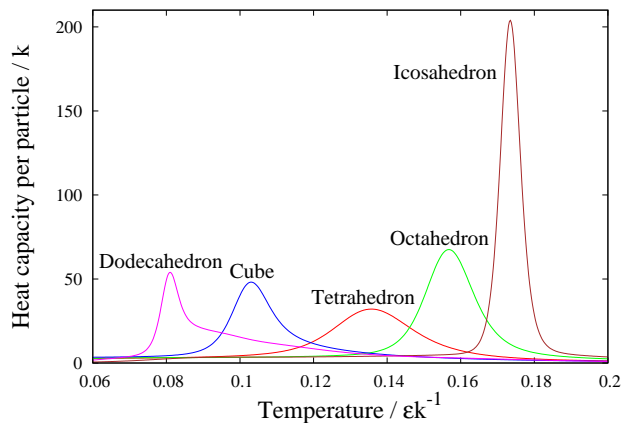


FIG. 5: (Colour Online) The heat capacity C_v as a function of temperature for each of the target structures at $\sigma = 0.45$. This data was obtained from equilibrium umbrella sampling simulations containing sufficient particles to form one target cluster, and so will differ somewhat from bulk values because of finite size effects.

There are two main target-dependent factors determining the value of T_c . Firstly, the number of patches per particle m is important, since the more patches are present the more the cluster gas is stabilised. The value of n , the number of particles per cluster, has the converse effect. When N particles assemble into N/n clusters there is a reduction in the effective number of particles in the system, and hence a corresponding reduction in the translational entropy. We can therefore obtain a crude estimate for T_c , neglecting vibrations and the mass dependence of effective ‘particles’, using

$$T_c = \frac{\Delta E}{\Delta S} \propto \frac{m}{1 - \frac{1}{n}}. \quad (8)$$

Table IIIB shows estimated values produced using this equation, along with values obtained from umbrella sampling simulations. Despite the extreme simplicity of the model used to derive Eqn. 8 it matches the data reasonably well, and provides an explanation for the ordering of the T_c values.

Lower values of T_c make assembly more difficult, by decreasing the potential range of T over which assembly might occur. It is noteworthy that cubes and dodecahedra have the lowest values of T_c , and are the hardest of our targets to assemble.

C. The cluster-liquid transition

For sufficiently large values of σ we see formation of aggregates associated with liquid-vapour coexistence, visible for all target structures in Fig. 3. We also see aggregates at low T and with narrower patches. The aggregates formed in these two regions are in fact strongly

Structure	m	n	Predicted C_v	Measured C_v
Tetrahedron	3	4	0.126	0.136
Cube	3	8	0.108	0.103
Dodecahedron	3	20	0.099	0.081
Octahedron	4	6	0.151	0.157
Icosahedron	5	12	0.172	0.173

TABLE I: Estimated T_c values, obtained from Eqn. 8 and from umbrella sampling simulations at $\sigma = 0.45$. The constant of proportionality in Eqn. 8 was chosen to give the best match to the data. Note that the simulations contained only enough particles to assemble one complete target structure in each case, and are therefore likely to give values slightly different to the bulk case.

related, with all properties varying smoothly between them. This is especially clear for the dodecahedral case, where there is no region of cluster formation separating the two regions of aggregate formation. All of the aggregates are associated with liquid-vapour separation.

Nevertheless, it is natural to divide these aggregates into two groups. In the first, at high σ , the aggregates are the stable state of the system. In general these thermodynamic aggregates have some liquid-like characteristics, being fairly compact and undergoing constant rearrangement. The second group of aggregates, those found at low temperature and lower σ , are metastable, with the target cluster being the true stable state. These kinetic aggregates display more glassy properties, often forming extended networks of string-like formations, which may percolate.

All of the aggregates tend to have irregular forms. Their surface tensions tend to be low, because so long as all patches are pointing inwards there is very little surface energy. As a result there is little drive towards forming spherical droplets. At low values of σ the surface tension falls even further since there is no possibility of patches forming more than one bond. This, combined with a reduced ability to rearrange, leads to the formation of increasingly irregular and ramified aggregates at low σ . The energy of the aggregates tends to become less negative as well, since increasingly glassy systems are less able to optimise their configurations to find lower energies. This effect is visible in Fig. 6, which shows the final energies of simulations over a range of T and σ for each of the target structures.

The structures of the aggregates also have a strong dependence on the target. At temperatures and patch widths close to those where target clusters are formed, the local structure within the aggregates tends to have a strong similarity to that in the target cluster, so that icosahedron-like groups are visible in the aggregates of icosahedron-forming particles, and so on. These structural similarities are visible in Fig. 7, which shows snapshots of liquid aggregates near to the region of successful assembly. The one target which consistently produces aggregates with little resemblance to the target struc-

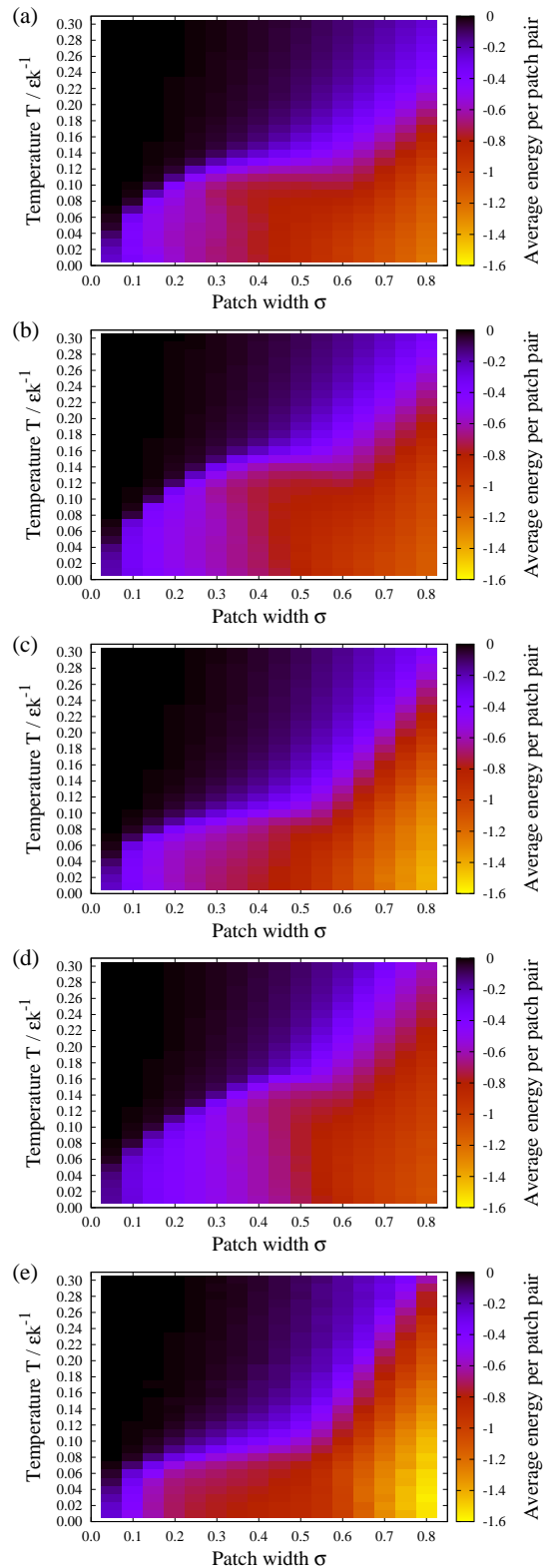


FIG. 6: (Colour Online) The normalised final total energy $\frac{E}{2Nm}$ (where Nm is the total number of patches in the system) of systems of particles designed to form (a) tetrahedra, (b) octahedra, (c) cubes, (d) icosahedra, and (e) dodecahedra, for the same simulations as Fig. 2. The energy is normalised such that a value of -1 indicates that, on average, all patches are involved in one perfect bonding interaction. More negative values indicate that some patches are involved in more than one interaction, which is possible at high patch widths. The white lines again show the thermodynamic transition temperature T_c for the transition from a gas of clusters to a gas of monomers, calculated for a one-cluster system (see Section III B).

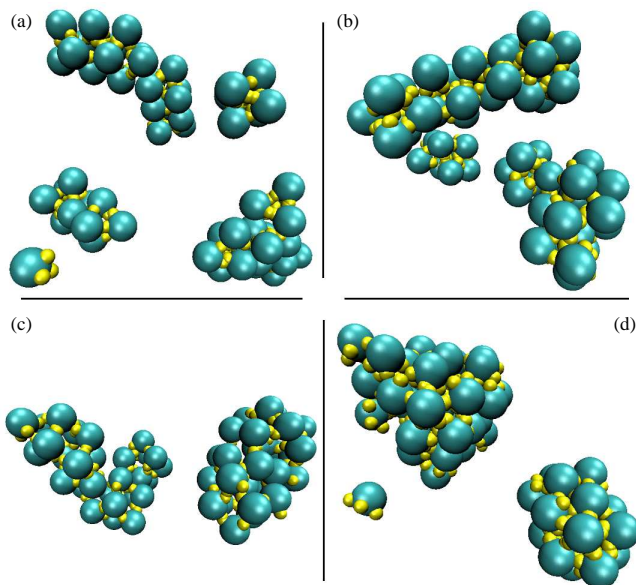


FIG. 7: (Colour Online) Typical configurations for parameters lying in the liquid regime but close to the region of successful assembly, for particles designed to form (a) tetrahedra at $T = 0.06$, $\sigma = 0.65$, (b) octahedra at $T = 0.09$, $\sigma = 0.65$, (c) cubes at $T = 0.08$, $\sigma = 0.55$ and (d) icosahedra at $T = 0.16$, $\sigma = 0.6$. Each simulation contains 60 particles at a number density of $0.15 \sigma_{LJ}^{-3}$.

ture is the dodecahedron. The wide splay angle (i.e. the angle between the patches and the symmetry axis) allows the formation of a wide variety of structures, resulting in highly ramified structures containing many hexagons and larger rings as well as pentagons (see Fig. 14). However as we move to higher values of σ the differences between the aggregates formed for the different targets are lost, so that the dense aggregates formed at very high σ look essentially the same for all cases.

Fig. 8 shows typical kinetic aggregate structures for tetrahedra, octahedra, cubes and icosahedra. Dodecahedral aggregates are shown later, in Fig. 14. We can see that all of the kinetic aggregates have a tendency to form chain-like structures. In larger simulations these may sometimes connect together and percolate across the simulation box. The local structure of the chains is again heavily dependent on the target structure, reflecting the symmetries of the target. We can also see that the tetrahedra have a greater tendency to form a number of smaller aggregates, which is consistent with Fig. 3. The narrow splay angle of the tetrahedron-forming particles promotes high curvature and hence small clusters. This effect is lost at higher σ , as the patch positions begin to have less control over aggregate structure.

The extent of the regions in which aggregates are found is important, as it sets boundaries on the region in which the target structure may successfully be formed. Here we will deal with the factors affecting the region in which liquid aggregates are stable, while in Section IIID3 we

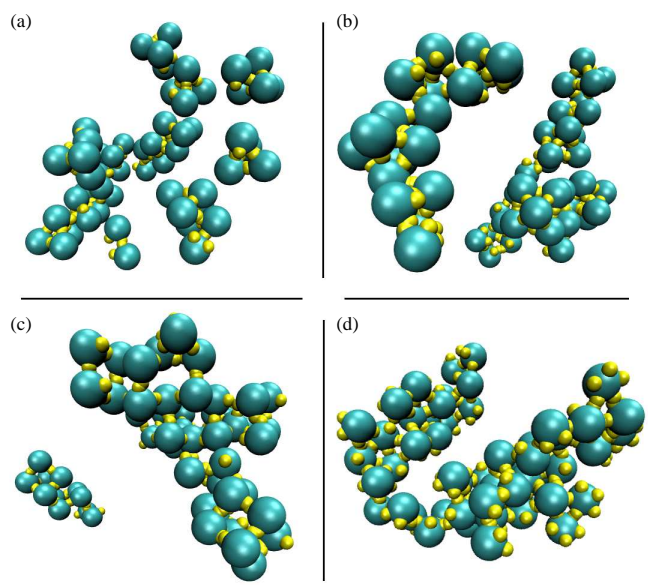


FIG. 8: (Colour Online) Typical configurations in the kinetic aggregation regime, for particles designed to form (a) tetrahedra at $T = 0.05$, $\sigma = 0.35$, (b) octahedra at $T = 0.07$, $\sigma = 0.35$, (c) cubes at $T = 0.06$, $\sigma = 0.4$ and (d) icosahedra at $T = 0.08$, $\sigma = 0.35$. Each simulation contains 60 particles at a number density of $0.15 \sigma_{LJ}^{-3}$.

will return to consider those determining the extent of the kinetic aggregate region.

It is useful to define some terms to describe the position of the transition from the cluster phase to the liquid at high σ . We define σ_c^{\max} and σ_l^{\min} as the maximum value of σ at which the cluster phase is found (which will be at zero temperature) and the minimum value of σ at which the liquid phase is found respectively. These two points are connected by the transition line T_{cl} . All three are shown in Fig. 4. σ_c^{\max} depends entirely on the energies of the two states since it is found at zero T , while the gradient of T_{cl} depends on the entropy difference between the two states.

Fig. 6 shows that the dodecahedra- and cube-forming particles are the most able to satisfy their patchy interactions in liquid droplets, and attain the greatest bonding energies. The low number of patches per particle m and the wide angles between patches result in fewer constraints of the liquid structure, making it easier to optimise patch-patch interactions. We can see a clear correlation between the angles between patches and the energy of the liquid. For the tetrahedra, octahedra and icosahedra, with angles between patches of 60° , the particles would be required to pack very closely together in order to satisfy all their bonds, and in fact we see relatively low bonding energies per patch. As we increase the angle, to 90° for cubes and then 108° for dodecahedra, the energy per patch steadily increases.

The entropy of the liquid aggregates might be expected to be correlated with the energy. When there are fewer

constraints it is not only easier to satisfy patch-patch interactions in a disordered configuration, but there are more ways of doing so, leading to a higher configurational entropy. We would therefore expect particularly high aggregate entropies for the dodecahedra and cubes.

We can obtain some limited information about the relative entropies of the aggregate and cluster phases by considering T_{cl} . The shallower the gradient of T_{cl} the greater the entropy differences between the aggregate and cluster phases, with negative gradients indicating that the aggregate is more entropically favourable. Unfortunately there is no clear approach for finding precise values for T_{cl} , but we can get an impression from Fig. 3. From those plots we can see that T_{cl} has a negative gradient for octahedra, icosahedra and probably cubes, indicating that the liquid has a higher entropy than the cluster gas, and hence that the disorder in the liquid more than compensates for the loss of translational degrees of freedom on forming a large aggregate. The gradient is less clear for tetrahedra and dodecahedra, although we would expect more closely similar entropies for tetrahedra since, as the smallest of the targets, the tetrahedral clusters are the most entropically favourable. Later (see Sec. III E) we show that T_{cl} has a far shallower slope for dodecahedra, such that σ_l^{\min} lies towards the left of the diagram. This is consistent with our expectations based on the dodecahedron's low aggregate energy and large cluster size.

D. Mechanisms of assembly and misassembly

The dynamics of the self-assembly simulations depend strongly on temperature and on the target. Fig. 9 shows the yields of each of the target structures as a function of T and time, at $\sigma = 0.45$. These plots show a number of interesting features.

Firstly, in each case the yield approaches equilibrium most rapidly at high temperatures, close to T_c . Here the dynamics are fast, and since liquid-like aggregates are not stable with respect to the monomer gas at these temperatures, the clusters face no competition. However, close to T_c the yield is limited by the finite width of the cluster gas-monomer gas transition. The transition has finite width because of the finite size of the clusters, with smaller clusters displaying a broader transition. This effect can be seen in Fig. 9 by considering the fall-off in yields at high temperatures, which is much sharper for icosahedra than for tetrahedra.

At slightly lower temperatures the assembly process becomes slower, since the timescale for rearrangement and the breaking of incorrect bonds is longer. As a result the temperature at which optimal yields are obtained decreases with time, being determined by the competition between rapid assembly at high temperatures and higher equilibrium yields at lower temperatures. Moving to still lower temperatures the yield on the timescale of our simulations falls off, until around T_g^{agg} it becomes severely limited. For target structures of tetrahedra, cubes and

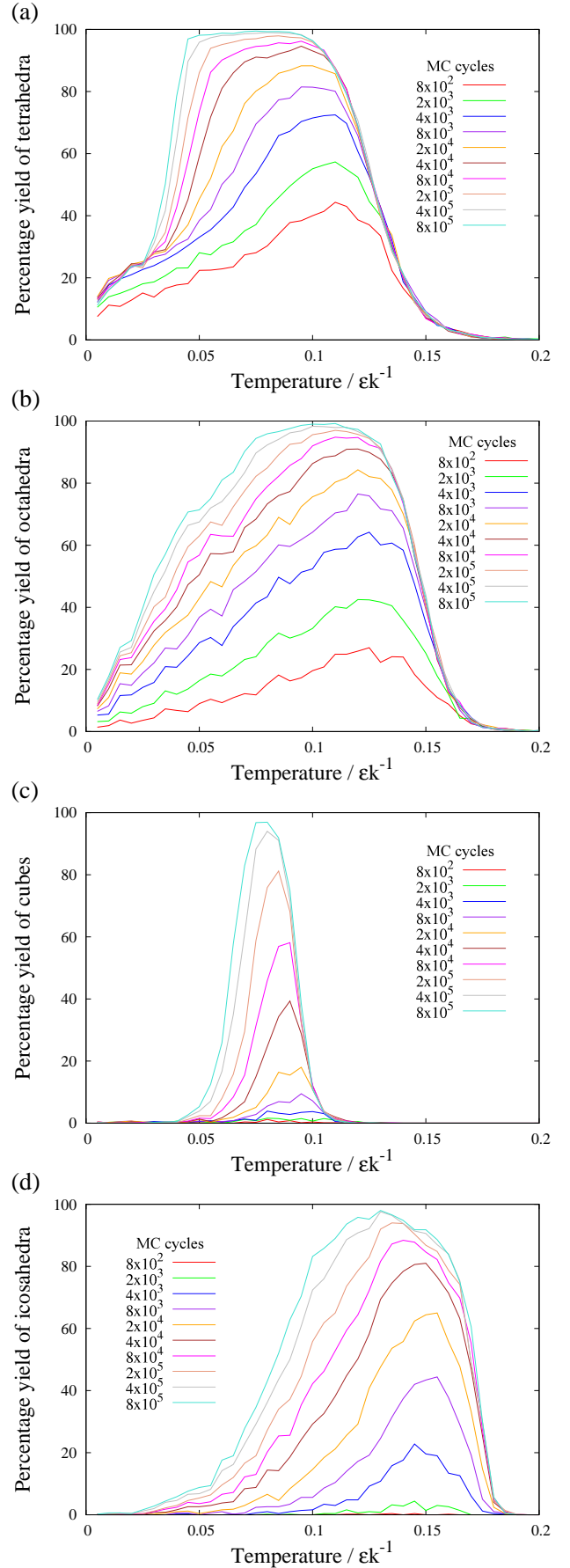


FIG. 9: (Colour Online) The yields of (a) tetrahedra, (b) octahedra, (c) cubes, and (d) icosahedra after different numbers of simulation steps as a function of temperature T , in simulations of systems of 1200 particles at $\sigma = 0.45$ and at a number density of $0.15 \sigma_{LJ}^{-3}$. Each data point is an average from five simulations.

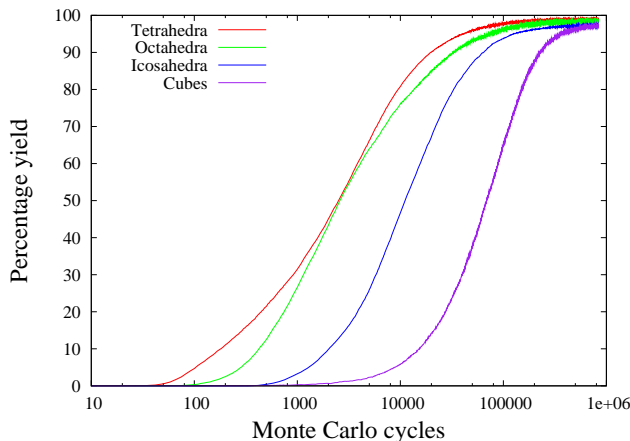


FIG. 10: (Colour Online) Yields as a function of time at optimal conditions for tetrahedra, octahedra, icosahedra and cubes, averaged over 100 simulations. The parameters used were $T = 0.09$, $\sigma = 0.4$ for tetrahedra, $T = 0.11$, $\sigma = 0.5$ for octahedra, $T = 0.14$, $\sigma = 0.45$ for icosahedra and $T = 0.08$, $\sigma = 0.45$ for cubes.

icosahedra, reasonably sharp cut-offs are seen at low T , giving approximate values for T_g^{agg} . In the case of the tetrahedra the yield does not fall to zero but rather to a finite value of around 20%, as some yield of tetrahedra is expected by straightforward chance assembly with no rearrangement required. Unlike the other targets, the plots for octahedra show an approximately linear decay in yields with decreasing temperature. The reasons for this are unclear.

Fig. 10 shows the yield as a function of time for each target structure, at the optimal conditions for the formation of that structure. While the final yields obtained in each case approach 100%, the time taken varies by almost two orders of magnitude. The order of the time taken for tetrahedra, octahedra and icosahedra is consistent with their relative sizes, with larger clusters taking longer to assemble as expected. Some tetrahedra form at very short times via the chance assembly mentioned above. However, the cubes take anomalously long to assemble. This is because at optimal conditions the cubes assemble via aggregation and rearrangement, a mechanism we will return to in Section III D 2. While effective, this mechanism is rather slow.

We will now consider in more detail the dynamics of assembly under three different temperature regimes: the regime where only the target clusters are stable, that where liquid-like aggregates are also stable with respect to the monomer gas, and finally low temperatures where the dynamics become glassy. Note that this discussion assumes a moderate value of σ ; at very low σ particles rarely feel each others' attractions and hence fail to assemble or aggregate, while at high σ the stable state is a liquid rather than a cluster gas.

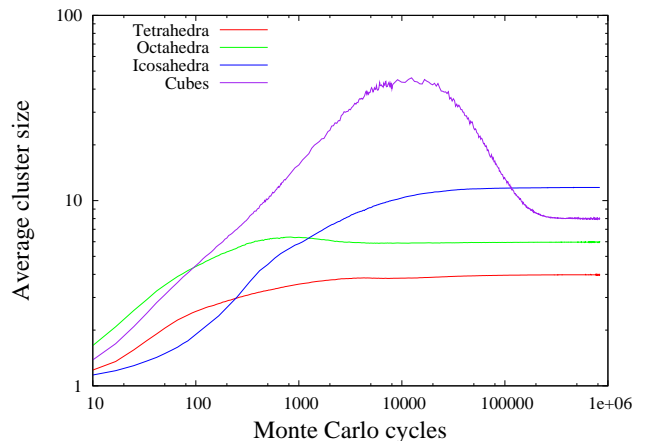


FIG. 11: (Colour Online) Average cluster sizes (weighted over particles) as a function of time at optimal conditions for tetrahedra, octahedra, icosahedra and cubes, averaged over 100 simulations. The parameters used were the same as for Fig. 10.

1. Target clusters stable, aggregates unstable: $T_{lv} < T < T_c$

In this regime the target cluster is the only structure stable with respect to the monomer gas. As a result assembly occurs entirely by addition of monomers and other small clusters, rather than proceeding via an aggregate state. Because aggregates are not stable there are essentially no competing states to the target structure.

Note that as this region is close to T_c , the yield may be constrained by the finite width of the cluster-monomer transition, i.e. the equilibrium yield of clusters may be significantly less than 100%. Lower temperatures will give a higher equilibrium yield.

In this region the speed of assembly is related to the size of the nucleation barrier and to the value of σ , with the dynamics becoming slower with decreasing σ due to the comparative rarity of bonding events between particles with narrow patches.

2. Both target clusters and aggregates stable: $T_g^{\text{agg}} < T < T_{lv}$

In this regime both the target clusters and large liquid aggregates are stable with respect to the monomer gas, leading to competition. However, mobility in the liquid droplets allows them to rearrange to form target clusters. Once complete clusters are formed all their patches point inwards, such that they experience very little attractive interaction with other particles. They are therefore able to “bud off”, separating from the rest of the liquid droplet in which they formed.

The optimal conditions for assembly are found in this regime, at a point in parameter space where the assembly mechanisms of monomer addition and of liquid aggrega-

tion followed by budding both operate. Fig. 11 shows the average cluster size against time under optimal assembly conditions for each of the target structures. For the cubes (and to some extent the octahedra) the average size passes through a maximum before falling to the target cluster size, indicating clearly that the mechanism of aggregation followed by rearrangement plays a very important role. The cube-forming particles have a marked tendency to aggregate (c.f. the low aggregate energies in Fig. 6) and so it is natural that their optimal assembly conditions should take heavy advantage of this mechanism. It seems from direct observation of simulations to also play a useful role for tetrahedra and icosahedra, but the dynamics of cluster formation and rearrangement are such that the average cluster size does not pass through a maximum in their cases.

3. Glassy regime: $T < T_g^{\text{agg}}$

T_g^{agg} is the temperature below which large clusters become unable to rearrange to form target clusters over the timescale of the simulation (and is therefore weakly dependent on timescale). It is reminiscent of a glass transition temperature. Below T_g^{agg} generally only large aggregates are formed, often forming extended ramified networks which may percolate.

T_g^{agg} is dependent on target geometry for a number of reasons. The first factor is the degree of order in the aggregates. Fig. 8 shows kinetic aggregates for target structures of cubes, icosahedra and dodecahedra. In the icosahedral case, the aggregates themselves contain a considerable degree of icosahedron-like structure, and only a relatively small amount of rearrangement is required for the aggregates to form complete clusters. For the cubic case a greater degree of rearrangement is required, while in the dodecahedral case, shown later in Fig. 14, the aggregates have very little dodecahedron-like structure at all, and would require almost total rearrangement to form the target clusters.

A second target-dependent feature is the size of the aggregates. In general a smaller splay angle in the assembling particles [make sure have defined this!] tends to lead to a higher surface curvature and hence to smaller aggregates. In Fig. 3 we can see that the low- T aggregates formed with tetrahedral and octahedra target structures are much smaller than for the other shapes.

A final factor is the size of the target structures themselves. Less rearrangement is needed to form a smaller target. Further, for smaller targets, the growth of aggregates is less likely to deviate significantly from the correct assembly pathway. For tetrahedra, some degree of successful assembly is observed even at very low T - simply by a chance, a significant proportion of groups of four particles coming together will assemble into tetrahedra. However, even for octahedra this effect becomes negligible.

E. The difficulty of assembling dodecahedra

Of the target structures examined in this paper, the dodecahedron is exceptional in the difficulty of its assembly. While the other challenging target, the cube, shows a restricted region in which assembly occurs, it is nevertheless easy to obtain high yields by conducting long simulations with carefully chosen parameters. By contrast dodecahedra are never formed with our model potential under any set of conditions.

In order to more fully understand the difficulty of assembling dodecahedra we attempted to obtain equilibrium thermodynamic data for a system of 20 particles, sufficient to assemble one dodecahedron. This was achieved only with considerable difficulty - indeed, the pathological difficulty of forming a single dodecahedron even using biasing techniques underlines the extreme unlikelihood of ever forming one under ordinary dynamics, and implies the presence of a large kinetic barrier to assembly.

Success was eventually achieved by combining two-dimensional umbrella sampling (using the number of bonds and the number of pentagons in the largest cluster as order parameters) with Hamiltonian exchange. Even with heavily biased umbrella sampling no dodecahedra were ever formed using the model potential that we have used throughout the rest of this paper, and it was found necessary to couple the simulation to an array of simulations which made use of an additional constraint in the potential to encourage assembly (see Section II B 4). Note that as these simulations were for systems large enough to form only a single cluster (20 particles, or 12 particles in icosahedral simulations performed for comparison) we expect finite size effects to have a significant effect, and the details of the data obtained will be different than for bulk systems. However, we expect the main features of the data to be unaffected.

In general, because of the low energy of the target structures, there exists for each target at moderate σ a temperature range over which the target is the only stable structure with regard to the monomer gas (see Section III D 1), so that aggregates can be formed only transiently and cannot compete with the target. One might expect that in this region at least, dodecahedra should be able to assemble. However, this is in fact not the case, since over most of the range of σ this region does not exist for dodecahedra. Fig. 12 shows a plot of the heat capacity C_v along with a plot of the average cluster size obtained from a Hamiltonian exchange simulation at a moderate patch width, $\sigma = 0.45$. The peak in C_v corresponds to T_c , the temperature below which clusters are stable. However, we can see that the average cluster size remains high beyond this point, indicating that the liquid aggregate state is in fact more stable at high temperatures than the cluster phase. The evaporation of this aggregate corresponds to the shoulder in the C_v plot.

This picture is confirmed in Fig. 13, which is obtained

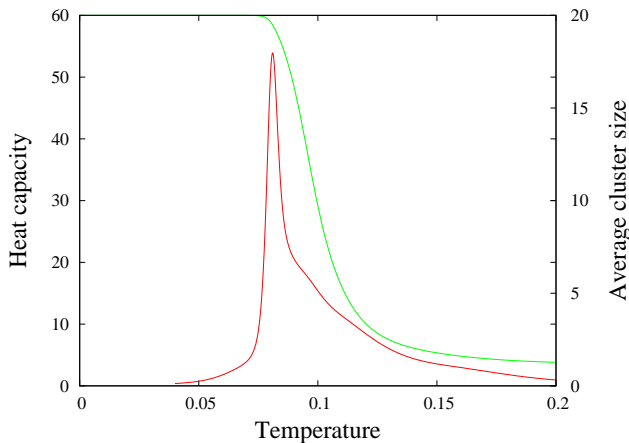


FIG. 12: (Colour Online) The equilibrium heat capacity C_v and average cluster size (weighted by particles) as a function of temperature for a twenty particle system of dodecahedron-forming particles, obtained using umbrella sampling and Hamiltonian exchange. The peak in the heat capacity corresponds to T_c , below which the stable state is a complete dodecahedron. The average cluster size remains high to a slightly higher temperature, showing that aggregates are present above T_c .

from Hamiltonian exchange simulations over a range of σ . The higher line in the figure shows the temperature at which the average cluster size in the box has a value of 10.5 (the midpoint of 1 and 20); although we cannot precisely measure T_{cl} , this line provides a fair approximation. The lower line is T_c . As was mentioned in Section III C, the entropy of the dodecahedral aggregates is very favourable compared to that of dodecahedra themselves, leading to a very shallow slope in T_{cl} . The two lines do not meet until around $\sigma = 0.2$, which we label σ_l^{\min} . So, for all values of σ higher than this, there is no region in which only dodecahedra are stable. At lower values of σ the assembly process is so hindered by the narrow patches that assembly is unable to occur. Note also that we expect that finite size effects will destabilise the aggregate, so that σ_l^{\min} would be even lower for the bulk system.

Given that at moderate σ the stable state of the system at higher temperatures is the aggregate, the only region in which dodecahedra might be able to form is at lower temperatures, where they represent the global free energy minimum. However, at low temperatures the system will aggregate very quickly, and would then need to rearrange to form a dodecahedron, a process which is severely inhibited by low temperature due to glassy behaviour. For the dodecahedral system though, rearrangement appears to be far more difficult than would be expected even allowing for temperature. This is probably a result of geometric factors which are unique, within our set of targets, to the dodecahedron. Because of the widely spaced patches on the particle surfaces, an enormous range of incorrect configurations are possible which

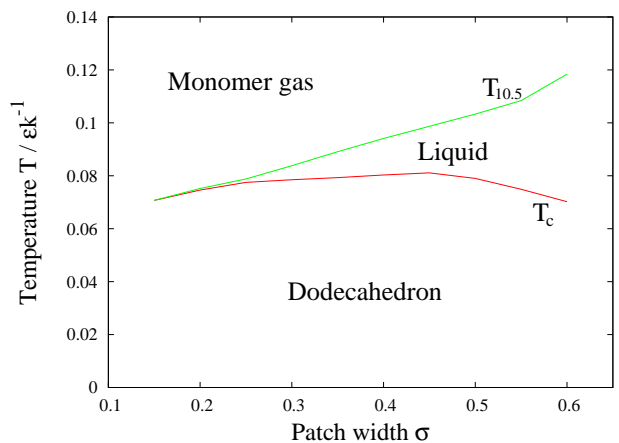


FIG. 13: (Colour Online) T_c and the temperature at which the average cluster size is 10.5, $T_{10.5}$, as a function of temperature for an equilibrium system of 20 dodecahedron-forming particles. $T_{10.5}$ gives an approximate value for the liquid-vapour transition, T_{lv} .

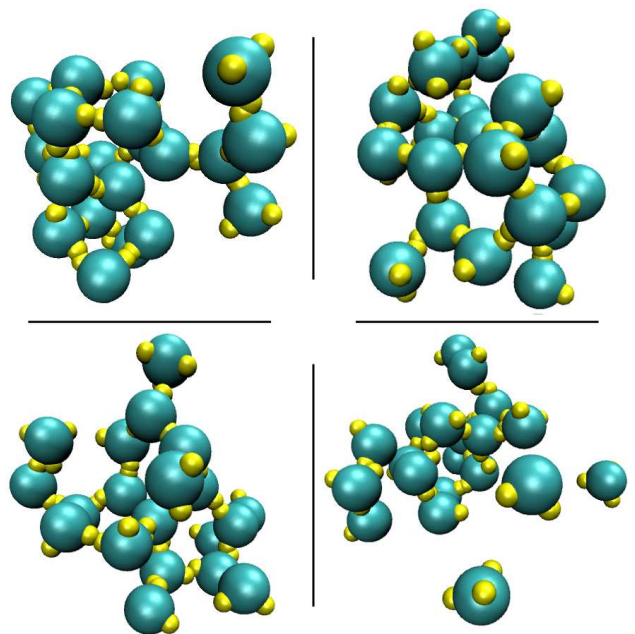


FIG. 14: (Colour Online) Four typical configurations for a twenty-particle system of dodecahedron-forming particles, all at $T = 0.09$ and $\sigma = 0.45$.

satisfy the bonding well, and which deviate significantly from the target structure even on a local scale. For example, pentagons are easily deformed into (non-planar) hexagons or larger polygons without introducing strain, and rings of particles are able to interpenetrate to form chain link-like structures. Fig. 14 shows a set of typical 20-particle aggregate configurations. These structures have little in common with correctly formed dodecahedra, and further, they experience little pressure to rearrange.

In order to obtain a clearer picture of the dynamics of the system, we made use of data from the Hamiltonian exchange simulations to plot free energy landscapes, both for icosahedra and dodecahedra. These plots are shown in Fig. 15. The icosahedral system provides a contrasting example of a successfully assembling system.

The first pair of plots, Fig. 15(a) and (b), show the free energy as a function of the number of particles and the number of correct polygons (triangles for the icosahedron and pentagons for the dodecahedron) in the largest cluster in the system. In Fig. 15(a), showing the landscape for an icosahedron, we can see clear free energy minima in two regions, representing the monomer gas and the icosahedron. Note that the monomer gas will typically contain at least one cluster of size three or four, which explains the position of the minimum. Between the two minima is a region of higher free energy, representing a transition state. Once the transition state is passed, the shape of the landscape directs the system towards forming an icosahedron, facilitating assembly (note that the high free energy state corresponding to a triangle count of 19 simply represents the fact that on forming the final bond a nascent icosahedron transitions in one step from having 18 to 20 triangles, and does not represent a barrier).

By contrast in Fig. 15(b), showing the landscape for a dodecahedron, there is little structure. There is no barrier to the formation of a 20-particle cluster, so the system will tend to rapidly aggregate, and will then experience little drive to form a dodecahedron. Indeed, if the system follows the steepest downhill path it will tend to form a single aggregate containing few pentagons, so that significant rearrangement would be needed to form a dodecahedron.

The second pair of plots, Fig. 15(c) and (d), show the free energy as a function of two different parameters, the configurational energy and a radial disorder parameter. The latter is in fact calculated as the standard deviation in the distance of particles from the centre of mass, and has a value of zero when all particles lie on a spherical shell (such as in the two target structures). Again, the plot for the icosahedron shows two valleys, corresponding to a monomer gas and to an icosahedron, separated by a transition state of higher free energy. Importantly, we see that in order to obtain lower energies the system is forced to steadily reduce its maximum radial disorder, such that it is directed into the icosahedral state. We also see that the free energy is a strong function of the radial order parameter.

By contrast, the free energy of the dodecahedral system appears to be almost entirely a function of the configurational energy, with very little dependence on the radial disorder. Energies close to that of the global minimum can be reached by highly disordered states. As a result the system is undirected, and experiences very little pressure towards forming an ordered cluster.

However, neither of the dodecahedral plots fully explain the situation. From these diagrams one might ex-

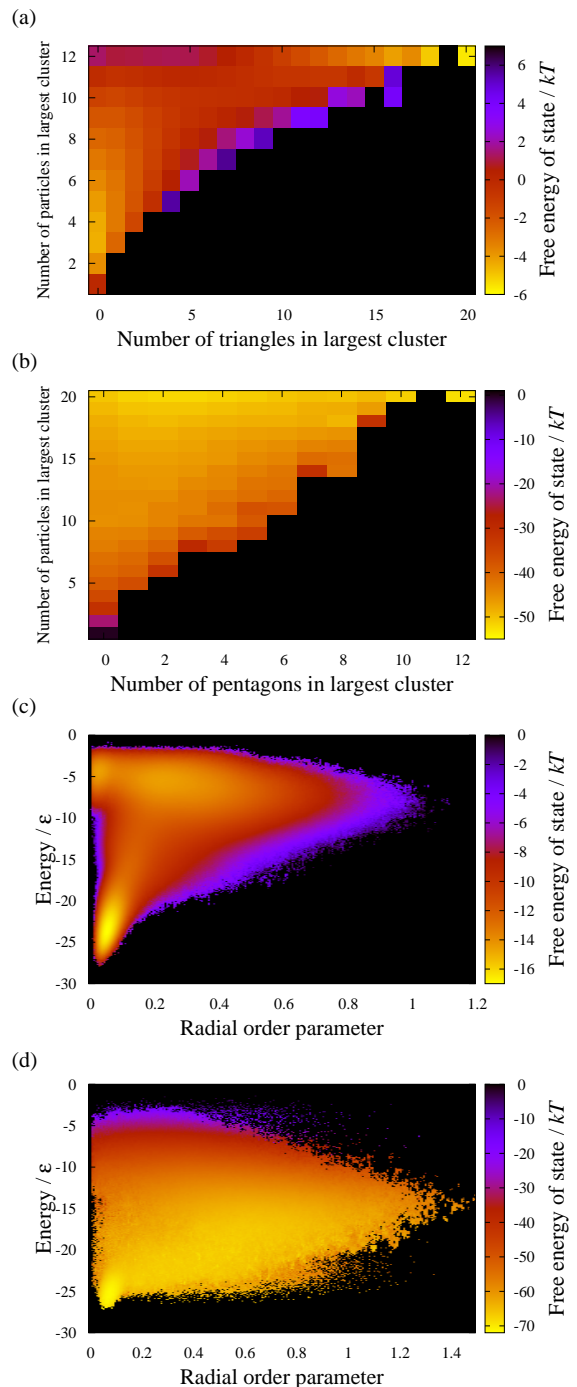


FIG. 15: (Colour Online) Free energy landscapes obtained from equilibrium simulations using umbrella sampling and, for the dodecahedral system, Hamiltonian exchange. (a) and (c) are for a system of 12 icosahedron-forming particles, while (b) and (d) are for a system of 20 dodecahedron-forming particles. (a) and (b) use the numbers of particles and rings in the largest cluster as axes, while (c) and (d) use the configurational energy and a measure of radial disorder, described in the text. The order parameters used to carry out the umbrella sampling were the numbers of bonds and triangles/pentagons in the largest cluster.

pect the formation of dodecahedra to be rare, but not essentially impossible. It appears that there is some large kinetic barrier preventing the formation of dodecahedra, which is not visible in these diagrams due to the choice of axes. Despite some effort, we were not able to find a combination of order parameters which would show this barrier explicitly.

To conclude, the pathological difficulty in assembling the dodecahedron arises from the combination of a number of subtle factors, but these factors themselves stem from very simple features in the target. The small number of patches per particle combined with the relatively large size of the target structure destabilize it in comparison to other target structures, preventing assembly at high temperatures where it might otherwise proceed more effectively. More importantly, the wide spacing of patches on the particles allows for the formation of high-entropy and low-energy aggregates with little structural similarity to dodecahedra, which provide such strong competition to dodecahedron formation as to essentially prevent it.

IV. GLOBAL TO-DOS

Extend T_c measurements for other sizes into liquid region to see when molten clusters appear \Rightarrow handle on T_{cl} ? (Perhaps unfair as greater finite size effects for n small. Or perhaps do it for roughly 20 particles in each case, i.e. 5 tetrahedra, 3 octahedra and so on; would need to modify bond count order parameter so it was the total bond count rather than the number of bonds in the largest cluster.)

Investigate what happens at low σ for all shapes.

V. CONCLUSIONS

We have presented a study of the self-assembly of a class of simple targets, the platonic solids, using a minimal model of assembling patchy particles. We have comprehensively mapped out the behaviours of systems of particles designed to form each of the targets as a function of temperature and patch width. Further, we have obtained equilibrium data using umbrella sampling and Hamiltonian exchange, allowing us to compare the thermodynamic properties of the different systems, and to produce free energy landscapes for the larger targets to elucidate the differences in their behaviour.

We find that the behaviour of the systems and the success of self-assembly are strongly dependent on the target structure. One key property which varies considerably between targets is the stability of disordered aggregates, which have a complex relationship with the self-assembly process. Over large regions of parameter space they act as competition and prevent successful assembly, but in other regions assembly may proceed by first forming aggregates which then rearrange to “bud

off” the target structures. As a result the assembly of cubes, whose constituent particles form particularly stable aggregates, is dominated by this budding mechanism, while dodecahedron-forming particles form aggregates so stable that they effectively block assembly of dodecahedra. In general we find that the stability of aggregates relative to the target clusters is determined largely by the spacing between the patches on the particles’ surfaces. Wider patch spacing leads to fewer constraints on the structures that the aggregates can adopt while satisfying all the patchy interactions, which in turn leads to both lower energies and higher entropies.

The stability of the target clusters themselves also varies considerably between targets, and depends both on the number of interactions each particle participates in, and on the size of the cluster. Greater size tends in general to decrease stability, but in fact the icosahedron is the most stable of our target structures since each particle interacts with five neighbours. High stability is a desirable trait as it allows assembly at high temperatures (corresponding to weak interactions), which lead to rapid breakup and rearrangement of misformed structures.

We find that the dependence on shape can be such that certain shapes never assemble successfully; dodecahedra appear to be essentially impossible to correctly assemble in our model. The dodecahedron is a relatively unstable target because of its small number of interactions (each particle having only three nearest neighbours) and large size. The aggregates with which it competes, by contrast, are exceptionally stable. As a result at moderate patch widths the aggregates are stable to higher temperatures than the dodecahedra, and indeed there is no region of parameter space where the dodecahedron is both thermodynamically stable and kinetically accessible.

These observations collectively suggest a number of design rules for targets that will assemble easily. Firstly, a high number of nearest neighbours allows for more interaction which stabilise the target structure. Secondly, closely spaced patches serve to inhibit the formation of stable aggregates which can provide competition. These two features can be combined by choosing shapes with triangular faces, and as such we would argue that triangular faces are a major advantage in any target structure.

Proceeding to larger and more ambitious self-assembly targets, a difficulty arises. As the target size increases, the competition between the target and disordered aggregates increasingly favours aggregates, as the targets become less entropically favourable. This suggests limits to the size and complexity of targets of monodisperse self-assembly which can be successfully formed using the simple interactions we have used here. A natural approach to this difficulty would be to introduce further constraints to the potential. In particular a potential including torsional constraints, i.e. one in which the interactions are specific both in direction and in relative orientation, would massively reduce the number of competing configurations available. Protein-protein interactions have this kind of specificity, and we expect that this

is crucial in the assembly of large structures such as virus capsids. We examine the effect of using such a modified potential in the accompanying paper.

Are we still grateful to the Royal Society?

Acknowledgments

The authors are grateful for financial support from the EPSRC and the Royal Society.

* Authors for correspondence

¹ M. F. Hagan and D. Chandler, *Biophys. J.* **91**, 42 (2006).

² R. L. Jack, M. F. Hagan, and D. Chandler, *Phys. Rev. E* **76**, 021119 (2007).

³ M. F. Hagan, *Phys. Rev. E* **77**, 051904 (2008).

⁴ O. M. Elrad and M. F. Hagan, *Nano Lett.* **8**, 3850 (2008).

⁵ H. D. Nguyen, V. S. Reddy, and C. L. Brooks III, *Nano Lett.* **7**, 338 (2007).

⁶ T. Q. Zhang and R. Schwartz, *Biophys. J.* **90**, 57 (2006).

⁷ T. Q. Zhang, W. T. Kim, and R. Schwartz, *NanoBioscience, IEEE Tran. on* **6**, 235 (2007).

⁸ B. Sweeney, T. Q. Zhang, and R. Schwartz, *Biophys. J.*

94, 772 (2008).

⁹ N. Misra, D. Lees, T. Q. Zhang, and R. Schwartz, *Comp. and Math. Meth. in Med.* **9**, 277 (2008).

¹⁰ D. C. Rapaport, *Phys. Rev. Lett.* **101**, 186101 (2008).

¹¹ F. Romano, P. Tartaglia, and F. Sciortino, *J. Phys.: Condens. Matter* **19**, 322101 (2007).

¹² F. Sciortino, *Euro. Phys. J. B* **64**, 505 (2008).

¹³ A. W. Wilber, J. P. K. Doye, A. A. Louis, E. G. Noya, M. A. Miller, and P. Wong, *J. Chem. Phys.* **127**, 085106 (2007).